second symmetric state) for the infinite-height well, and compare it with the corresponding values obtained from the numerical solution for the finite-height well. (You will need to use a numerical root solver.) For the finite-height well, assume barrier height $V_0 = 0.3$ eV, which is $\Delta E_C = E_C^{Al_\alpha Ga_{1-\alpha}As} - E_C^{GaAs}$ for $\alpha = 0.3$. Comment on the appropriateness, at least for low energy states, of the much simpler infinite well model.

9. Assume a hard-wall model of a rectangular cross-section metallic quantum wire. If the wire is 1 nm thick and 10 nm wide, determine how many subbands are filled at 1 eV.

10. In a quantum wire, the available energy gets partitioned into various channels (subbands). Is this partitioning unique?

11. Calculate the energy levels in a quantum dot in the form of a cube, 5 nm on a side. Assume zero potential energy in the dot, and an infinitely high potential bounding the dot. Assume that $m^* = 0.045m_e$ in the dot material.

12. How small must a metal nanosphere be in order for the ground state energy to be 1 eV? Assume a hard-wall model.

13. Consider a hard-wall model of a cubical metal quantum dot, having side length $L = 3$ nm. What is the energy of a transition from the (1, 1, 1) state to the (2, 2, 1) state?

14. Consider a CdS quantum dot, having $E_g^{bulk} = 2.4$ eV, $m_e^* = 0.21m_e$, $m_h^* = 0.8m_e$, and $\varepsilon_r = 5.6$. What is the expected peak absorbance energy (E_g^{dot}) and wavelength for a $R = 2$ nm dot? Repeat for a $R = 3$ nm dot.

15. Using the Internet, find a company that sells quantum dots for biological and/or medical applications, and write a one-half to one page summary of one of their products, and its applications.

16. There is significant debate about the possible adverse health effects of quantum dots in biological bodies. Much, but not all, of the concern revolves around the use of cadmium in quantum dot structures. Write a one page summary of the debate, including the benefits and drawbacks of using quantum dots in living bodies.

17. Determine quantum dot applications to lasers, and write a one-half to one page summary of the uses, pros, and cons, of using quantum dots as lasing materials.

Chapter

10

NANOWIRES, BALLISTIC TRANSPORT, AND SPIN TRANSPORT

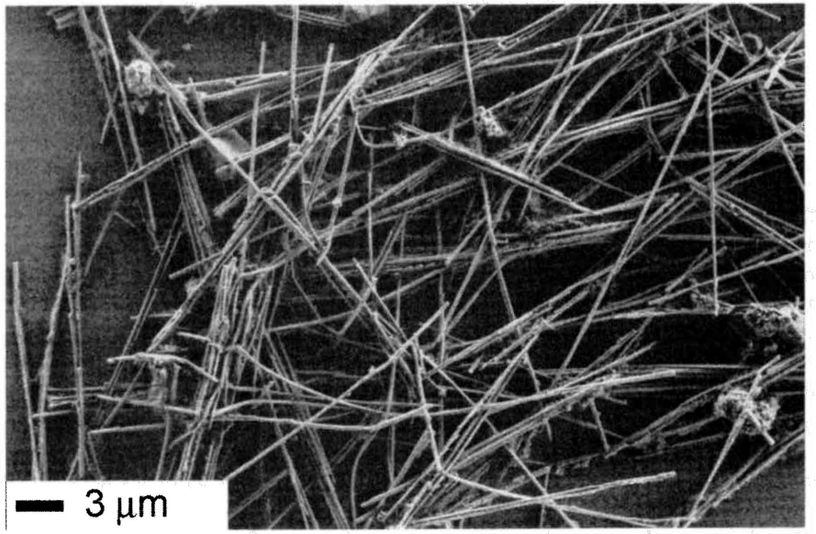

SEM image of 200 nm diameter nickel nanowires. Ann Bentley & Professor Art Ellis, Materials Science and Engineering Department, University of Wisconsin-Madison. Image courtesy the Nickel Institute.)

In an ordinary electrical circuit, conducting wires are used to interconnect electrical devices. For example, common residential wiring typically consists of 12 and 14 gauge[†] round cross-section wire, having diameters of 2.05 mm and 1.63 mm, respectively. Discrete electronic circuits built on a breadboard typically use 22 gauge wire, having a diameter of 0.64 mm. Integrated circuits use printed interconnects, having roughly rectangular cross sections, with typical widths on the order of 0.16 μm, and thicknesses on the order

[†]Americal Wire Gauge, AWG.

of 0.25 μm, although these dimensions continue to shrink along with transistor feature size.[†]

As electronics shrink, the "wires" used to interconnect devices obviously must also shrink in size. In this chapter, we consider what happens to the concept of conductivity when the dimensions of the conductor are very small. In this regard, there are two important dimensions to consider: the wire's radius, and its length. When the wire's radius is very small, on the order of the Fermi wavelength, we have a quantum wire, as discussed previously (Sections 4.7.2 and 9.2). Transport occurs axially along the wire, in well-quantized transverse energy subbands. We will discuss this topic further in this chapter.

However, we have not considered the case when the length of the conductor in the direction of propagation is "small." This topic not only is relevant to wire interconnects, but also is, for example, of interest in considering the channel of a FET, as channel lengths become a few nanometers. As we will see, this case leads to the concept of *ballistic transport*, which is a uniquely nanoscale phenomenon. The chapter concludes with a discussion of *spin transport*, and the possible applications of spin in forming devices.

10.1 CLASSICAL AND SEMICLASSICAL TRANSPORT

10.1.1 Classical Theory of Conduction—Free Electron Gas Model

Consider a solid material. The electrons (and the atoms themselves) are in a continual state of vibration, and temperature T is a measure of the energy associated with this motion. Considering that a particle has three degrees of freedom in which to move (x, y, and z), we see that Boltzmann's law states that each particle has thermal energy

$$E_T = \frac{3}{2}k_B T \tag{10.1}$$

joules, where k_B is Boltzmann's constant ($k_B = 1.38 \times 10^{-23}$ J/K). This is actually only true for gases, but is a reasonable approximation for many solids. For a particle having mass m and moving at an average velocity v in the absence of a potential field, the total energy (kinetic) is $mv^2/2$, and so

$$\frac{1}{2}mv^2 = \frac{3}{2}k_B T, \tag{10.2}$$

where v is the *mean thermal velocity* of electrons. Solving for velocity, we obtain

$$v = v_T = \sqrt{\frac{3k_B T}{m}}. \tag{10.3}$$

At absolute zero,[‡] $v_T = 0$, and at room temperature (293 K), for an electron this gives

$$v_T = 1.15 \times 10^5 \text{ m/s}. \tag{10.4}$$

[†]For integrated circuits, the thickness/width ratio is kept relatively large to keep interconnect resistance at a reasonable level.

[‡]As an aside, at $T = 0$ K, classical theory predicts that all motion stops, whereas quantum theory dictates some nonzero energy; atoms are in their ground state, analogous to the ground state particle-in-a-box result (4.53).

However, this motion is random and does not result in any net current, and so we'll denote this velocity as a scalar quantity.

Now consider applying a voltage for a time t across a solid containing free electrons. The resulting electric field accelerates the electrons in the direction opposite to that of the applied field ($\mathbf{F} = q_e\mathbf{E}$ and $q_e = -e = -1.6 \times 10^{-19}$ C), and, treating the electrons as classical particles, we find that Newton's law gives

$$\mathbf{F} = m_e\mathbf{a} = m_e\frac{d\mathbf{v}}{dt} = q_e\mathbf{E}, \tag{10.5}$$

where $\mathbf{E}$ is the vector electric field. This results in

$$\mathbf{v}(t) = \int_0^t \left(\frac{q_e}{m_e}\mathbf{E}\right) dt = \frac{q_e t}{m_e}\mathbf{E} = \mathbf{v}_d(t), \tag{10.6}$$

where we have assumed that $\mathbf{E}$ is independent of time. Note that this velocity is the component of velocity due to the applied electric field, which is called the *drift velocity*. Therefore, the total velocity of an electron in an applied field is the sum of the thermal and drift velocities,

$$\mathbf{v} = \mathbf{v}_T + \mathbf{v}_d, \tag{10.7}$$

where $\mathbf{v}_T$ is randomly directed.

However, the result (10.6) predicts that the electrons will increase their velocity indefinitely as time increases, which is obviously not true.[†] The problem is that collisions between the accelerated electrons and the material lattice (Chapter 5) have not been taken into account.[‡] It is these collisions that result in energy transfer from the applied field $\mathbf{E}$ to the material, via the electrons, that results in heating of the material. The mean time between collisions is τ, called the *relaxation time* (sometimes called the *momentum relaxation time*).

A good way to account for these collisions is to adjust the integral in (10.6), keeping in mind the model of electrons accelerating from $t = 0$ until they collide with something (a lattice imperfection, a thermal vibration, etc.) at $t = \tau$. Since the lattice atoms are much heavier than the electrons, it is assumed that each collision results in the electron completely losing its momentum[§] gained from the applied field. Therefore, in (10.6), we integrate from $t = 0$ to $t = \tau$, obtaining

$$\mathbf{v}_d = \frac{q_e\tau}{m_e}\mathbf{E}. \tag{10.8}$$

[†]For a particle in a vacuum this is closer to the truth, although relativistic effects limit the velocity.

[‡]As discussed in Chapter 5, an electron can move freely through a perfect periodic lattice, without scattering, and assuming that the electrons' energy is in an allowed energy band. However, that is a quantum result, and here we are discussing the classical model, and even in the quantum model, electrons will collide with lattice imperfections, or lattice vibrations (phonons). So, for simplicity, here we will just say that the electron collides with "the lattice."

[§]In a more precise treatment, the mean time between collisions and the momentum relaxation time are different, since a collision may not result in the complete loss of momentum.

We then have

$$\mathbf{v}_d = -\left(\frac{e\tau}{m_e}\right)\mathbf{E} = -\mu_e \mathbf{E}, \tag{10.9}$$

where μ_e is called the electrical *mobility* of the material, with units of m^2/V-s. Since mobility is proportional to the relaxation time, large mobility means that electrons travel a (relatively) long distance before colliding with the lattice.

We can consider τ as a temperature-dependent material parameter that can be measured, and, thus, $\mathbf{v}_d$ can be determined. As an example, if $\tau = 2.47 \times 10^{-14}$ s (an approximate value for copper at room temperature), and $|\mathbf{E}| = 1$ V/m, then $v_d = 4.35 \times 10^{-3}$ m/s, which is much less than the thermal velocity. Therefore, in the classical model, we view electron movement as being made up of rapid ($\sim 10^5$ m/s), random thermal motion, superimposed on much slower ($\sim 10^{-3}$ m/s) directed movement in the presence of an applied field or potential. Note, however, that despite the small value of drift velocity, electrical signals propagate as electromagnetic waves at the speed of light in the medium in question (e.g., $c \simeq 3 \times 10^8$ m/s for air). For highly conducting wires, the electromagnetic wave associated with the electrical signal carried by the wire propagates in the medium exterior to the wire (often air, or some dielectric insulation) even though in the wire itself, the electrons travel at a significantly slower velocity.

The total number of electrons crossing a unit plane each second is $N_e \mathbf{v}_d$, where N_e is the number of electrons per unit volume (i.e., the electron density, m^{-3}). The classical current density is obtained as

$$\mathbf{J} = q_e N_e \mathbf{v}_d = q_e N_e \left(\frac{q_e \tau}{m_e}\mathbf{E}\right) = \frac{q_e^2 \tau}{m_e} N_e \mathbf{E} \ \text{A/m}^2, \tag{10.10}$$

often written as Ohm's law,

$$\mathbf{J} = \sigma \mathbf{E}, \tag{10.11}$$

where

$$\sigma = \frac{q_e^2 \tau}{m_e} N_e \tag{10.12}$$

is called the *conductivity* (S/m $= 1/\Omega$m). Large conductivity can result from large mobility, large electron density, or both. The conductivity (10.12) holds for a wide range of materials, although for semiconductors the effective mass should be used in place of m_e. In this case, mobility is defined by

$$\mu_e = \frac{e\tau_e}{m_e^*}, \qquad \mu_h = \frac{e\tau_h}{m_h^*} \tag{10.13}$$

for electrons and holes, respectively, where $\tau_{e,h}$ is the appropriate relaxation time for electrons and holes. Therefore,

$$\sigma = q_e^2 \left(\frac{\tau_e}{m_e^*} N_e + \frac{\tau_h}{m_h^*} N_h\right). \tag{10.14}$$

In copper, one of the best electrical conductors, at room temperature

$$\sigma \simeq 5.9 \times 10^7 \ \text{S/m}, \tag{10.15}$$

using the electron density $N_e \simeq 8.45 \times 10^{28}$ /m^3 and $\tau = 2.47 \times 10^{-14}$ s. Therefore,

$$\mu_e \simeq \frac{\sigma}{eN_e} = 4.35 \times 10^{-3} \ \text{m}^2\text{V}^{-1}\text{s}^{-1}, \tag{10.16}$$

leading to

$$\mathbf{v}_d = -\mu_e \mathbf{E} \simeq -4.35 \times 10^{-3} \ \text{m/s} \tag{10.17}$$

as previously stated for a one volt per meter electric field.

10.1.2 Semiclassical Theory of Electrical Conduction—Fermi Gas Model

The preceding *classical* model (called the *Drude model*) is simply a classical free electron gas model with the addition of collisions. Of course, it is better to use quantum physics principles. Rather than the thermal velocity, we should consider the Fermi velocity, which is the quantum velocity roughly analogous to the classical thermal velocity. By modifying Fig. 8.8 on page 273 to show momentum, rather than wavevector, we see that in the absence of an applied field, the Fermi surface associated with electrons in a bounded region of space is symmetric about the origin, as shown in Fig. 10.1.

All momentum states within the Fermi sphere are occupied, and those outside the Fermi sphere are empty.[†] Thus, for every occupied state $\mathbf{p}$, there is a state $-\mathbf{p}$, such that there is no net motion, analogous with the classical concept of thermal velocity being random.

From (8.47), the Fermi velocity is given by

$$v_F = \frac{\hbar k_F}{m^*} = \frac{\hbar \left(3N\pi^2\right)^{1/3}}{m^*} \tag{10.18}$$

[†]Of course, this is only strictly true at $T = 0$ K; for $T > 0$, the Fermi surface tends to become smeared out a bit, but the assumption of a sharp Fermi surface is a good approximation for even moderately large T, due to the behaviour of the Fermi-Dirac distribution.

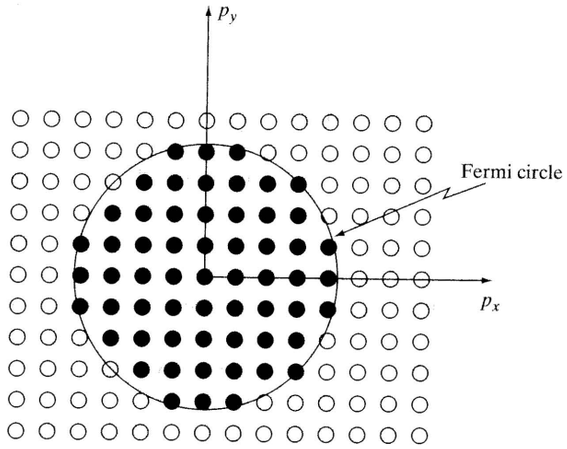

Figure 10.1 Electronic states in the momentum (p_x–p_y) plane for the case of a bounded region of space with no applied electric field. The states within the Fermi circle shown are occupied.

for the electron gas model of a metal, where N is the three-dimensional electron density. For metals, v_F is typically an order of magnitude larger than the thermal velocity. For example, for copper,

$$v_F = 1.57 \times 10^6 \text{ m/s}. \tag{10.19}$$

Therefore, the Fermi velocity is many orders of magnitude larger than the drift velocity, in general. As with the thermal velocity in the classical model, the motion due to the Fermi velocity is randomly directed. Therefore, electrons in a metal can often be considered to be moving randomly at the Fermi velocity in the absence of an applied field.

When we apply an electric field to a material, we will accelerate electrons, resulting in drift. Note that (10.8) for the drift velocity, and, hence, (10.10), is still approximately valid in this semiquantum model, even though they were derived using classical concepts. This can be understood because, as we are using τ here, it is a measured or empirical quantity, rather than being itself strictly derived from classical physics. Therefore, we obtain a somewhat empirical, although realistic model yielding good agreement with measurements.

In theory, τ in the classical model is the average relaxation time of all electrons (since in the free electron gas model, all electrons contribute to conduction), whereas in the quantum model, it is the relaxation time of electrons at the Fermi surface (i.e., the electrons most important for conduction). However, we don't need to be overly concerned with this detail here. The idea to keep in mind is that in going from the classical to the semiclassical model we are really replacing the thermal velocity with the Fermi velocity.[†] In either model, the net effect of applying an electric field, at least pertaining to the resulting current flow, is to consider the electrons to have directed movement at velocity $\mathbf{v}_d$.

[†]In addition, in the semiclassical treatment, rather than the collision-based model, we also consider Bloch's theorem, and the fact that electron scattering only occurs with impurities or lattice vibrations.

From the viewpoint of the Fermi surface, the energy or momentum gained by the electrons from the applied field can be obtained from[†]

$$\mathbf{F} = m^* \frac{d\mathbf{v}_d}{dt} = \frac{d\mathbf{p}}{dt} = \hbar \frac{d\mathbf{k}}{dt} = q_e \mathbf{E}, \tag{10.20}$$

and so the increase in momentum in a time increment dt is, using $\tau = dt$,

$$\delta \mathbf{p} = q_e \tau \mathbf{E}. \tag{10.21}$$

Thus, when an electric field is applied to the material, the Fermi surface is shifted from the origin, resulting in a nonzero net momentum, and electrical conduction, as shown in Fig. 10.2. That is, as shown in the figure, there are states having certain values of p_x that are not compensated for by states having $-p_x$, resulting in a net positive x-directed motion. When the applied field is removed, the Fermi surface shifts back (relaxes) to its previous position, symmetric about the origin.

This semiclassical theory of conduction, using the Fermi velocity rather than the thermal velocity, is called the *Fermi gas model*, in which electrons have total velocity

$$\mathbf{v} = \mathbf{v}_F + \mathbf{v}_d. \tag{10.22}$$

The formulas for conductivity, (10.12), and mobility are still used in this model.

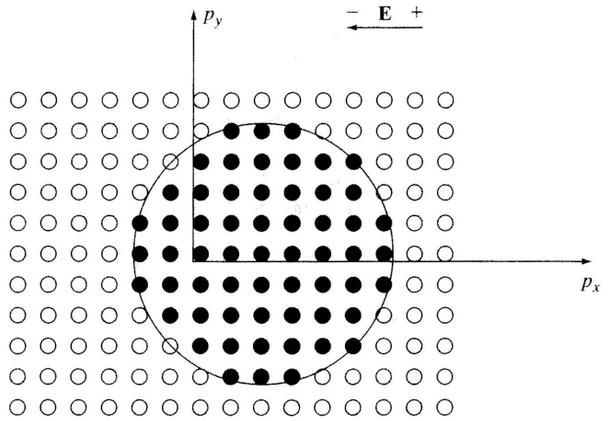

Figure 10.2 Electronic states in the momentum (p_x–p_y) plane for the case of an applied electric field, in which case the Fermi surface is shifted by the field. The states within the Fermi circle shown are occupied.

[†]As there are several different concepts of momentum described in the text, at the risk of being repetitive, it is worthwhile to be clear about what concept of momentum we are using. In (2.16), $\mathbf{p} = \hbar\mathbf{k}$ is the particle's actual momentum, and in Section 5.3.1, $\hbar\mathbf{k}$ is the crystal momentum, which is not the electron's physical momentum, but describes a Bloch electron's state. Here, because we are considering a Fermi gas model (no crystal lattice), $\mathbf{p} = \hbar\mathbf{k}$ represents the average physical momentum of electrons.

It is also convenient to define the *mean-free path* as the mean distance an electron travels before a collision with the lattice. This gives for copper

$$L_m = (v_d + v_F)\,\tau \simeq v_F\tau = 3.9 \times 10^{-8}\ \text{m}, \tag{10.23}$$

which indicates that the electron scatters off the lattice infrequently, since the mean free path is on the order of 100 lattice constants. (The lattice constant for copper is 3.61 Å.) Using the thermal velocity alone (i.e., the classical model), one obtains

$$L_m = 2.8 \times 10^{-9}\ \text{m}, \tag{10.24}$$

which is approximately eight lattice constants. Thus, using the thermal velocity, we would expect that the electron should scatter from the lattice quite frequently. This would also seem to make physical sense in the classical view, as we picture a dense sea of electrons moving through and colliding with the lattice. However, using the (better) Fermi velocity and the semiclassical model, we see that electrons actually scatter from the lattice infrequently. This is consistent with the fact that quantum mechanics predicts that an electron can pass through a perfect periodic lattice without scattering, where the effect of the lattice merely leads to the use of an effective mass, as described in Section 5.3.1. As discussed previously, scattering actually occurs not with a perfect lattice, but at the sites of lattice imperfections, or with lattice vibrations (phonons). Thus, the long mean free path, much longer than the lattice constant, makes perfect sense. Last, we should note that in a classical model, collisions between electrons and the lattice seem to be purely deleterious, giving rise to resistance. However, in the more realistic quantum model, as described in Section 5.3.1, collisions with impurities and vibrations are vital for electrical conduction to take place, thwarting Bloch oscillation.

Mobility (and obviously τ) is a strong function of temperature. As temperature decreases, mobility increases due to diminished phonon scattering. At sufficiently low temperatures, phonon scattering is suppressed, and scattering is mostly due to impurities. For crystals of relatively pure copper at liquid helium temperatures (4 K), it is possible to obtain $\tau \sim 10^{-9}$ s. This results in

$$L_m = v_F\tau = \frac{\hbar\left(3N\pi^2\right)^{1/3}}{m^*}\tau \sim 0.003\ \text{m}, \tag{10.25}$$

using $N = 8.45 \times 10^{28}\ \text{m}^{-3}$ for copper. In this case, L_m is on the order of eight million lattice constants! This is obviously in agreement with Bloch's theorem from Chapter 5.

10.1.3 Classical Resistance and Conductance

In electrical circuit theory, resistance is defined by Ohm's law in circuit form,

$$R = \frac{V}{I}, \tag{10.26}$$

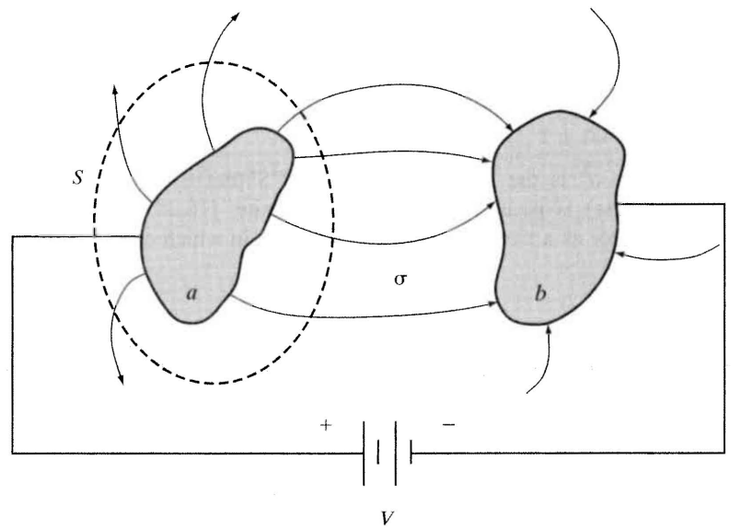

Figure 10.3 Geometry for the calculation of resistance between two conductors. The conductors are immersed in a material having conductivity σ. The arrows represent both electric field lines and electric current density, through $\mathbf{J} = \sigma\mathbf{E}$.

where V is the voltage across a circuit element and I is the resulting current that flows through the element. More generally, considering two arbitrarily shaped conductors immersed in a conducting medium characterized by conductivity σ, as shown in Fig. 10.3, the resistance between the conductors is

$$R = \frac{V}{I} = \frac{\int_a^b \mathbf{E}\cdot d\mathbf{l}}{\int\int_S \mathbf{J}\cdot d\mathbf{S}} = \frac{\int_a^b \mathbf{E}\cdot d\mathbf{l}}{\int\int_S \sigma\mathbf{E}\cdot d\mathbf{S}}. \tag{10.27}$$

The path a–b is any path from conductor a to conductor b, and S is any surface enclosing conductor a.

In particular, for a homogeneous rectangular solid having cross-sectional area $S = w_1 \times w_2$ and length L, we assume that the electric field $\mathbf{E}$ is uniform throughout the material and has magnitude $\mathcal{E}$, such that

$$R = \frac{\mathcal{E}L}{\sigma S\mathcal{E}} = \frac{L}{\sigma S}. \tag{10.28}$$

This is the three-dimensional result.

We are often interested in two-dimensional conductors, which are models of very thin metal strips, such as a printed circuit board interconnect. If $w_2 \to 0$, then (10.28) predicts that $R \to \infty$ (assuming that σ is finite). This result is true, however, we are often interested in the case of small yet finite values of w_2. For these situations, it is convenient to assume that a two-dimensional surface current density flows ($\mathbf{J}$ A/m), such that for a

two-dimensional flat wire having length L and width w,

$$R = \frac{V}{I} = \frac{\int_0^L \mathbf{E}\cdot d\mathbf{l}}{\int_0^w \mathbf{J}\cdot d\mathbf{S}} = \frac{\mathcal{E}L}{\sigma_s \mathcal{E} w} = \frac{L}{\sigma_s w}. \tag{10.29}$$

In this case σ_s is the *sheet conductivity* in S (not S/m). In a real material, where w_2 (the thickness) is perhaps very small, but finite, (10.28) applies, or we can model the thin conductor as a two-dimensional conductor, in which case (10.29) applies, where $\sigma_s = \sigma \times w_2$.

10.1.4 Conductivity of Metallic Nanowires—The Influence of Wire Radius

In the next section we will examine what happens when wire length L becomes extremely small relative to the mean free path, resulting in an interesting phenomenon that is not encountered in the world of macroscopic conductors. However, before considering this case, it is worthwhile to make some comments about the influence of wire cross-section size on conductivity.

Consider a circular cross-section wire having radius a and length L, and assume that L is very large compared to the mean free path (and, therefore, certainly to the Fermi wavelength as well). When a is macroscopic, one uses the model of conductivity for a bulk material, such as (10.12). In this case, the resistance is given by (10.28). For example, assuming a copper ($\sigma = 5.9 \times 10^7$ S/m) wire having radius $a = 10$ mm, $R = 5.395 \times 10^{-5}$ ohms/m. Thus, one would need approximately 18, 536 m of wire to amount to a resistance of one ohm, which is why we can often ignore wire resistance in electrical circuits. However, if $a = 10$ μm, $R = 53.95$ ohms/m, amounting to 1 ohm in only 1.85 cm. If $a = 10$ nm, the resistance is huge, $R = 5.395 \times 10^7$ ohms/m.

However, it is important to note that for wires having radius values on the order of the mean free path or less, the conductivity value is changed from the case of a bulk material. Thus, the previously listed values of resistance for the 10 mm and 10 μm radius wires are reasonable, although the value for the 10 nm radius wire is not large enough. For example, copper has a mean free path of approximately 40 nm, and in this range, radius-dependent effects are usually manifest. In fact, one may consider that radius-dependent effects may occur even when the radius is approximately double this value, on the order of 80–100 nm. In the 1–20 nm radius range, the conductivity of the wire certainly will differ appreciably from the bulk value, and generally the conductivity significantly decreases as a is reduced. This is due to several effects, such as scattering from the wire's surface and from grain boundaries, not to mention the difficulty in fabricating high-quality, defect-free metals at small size scales. Thus, as a very rough rule of thumb, one can use the bulk value of conductivity for many good conductors when the radius value is above approximately $a = 80$–100 nm. Below this point, down to radius values of perhaps 5–10 nm (but above metallic quantum wire dimensions), one may expect to need to use

a size-dependent value of conductivity, perhaps based on measurement. A relatively simple approximate formula for the resistivity (ρ; $\rho = \sigma^{-1}$) of rectangular cross-section wires is[†]

$$\rho = \rho_0 \left\{ \frac{1}{3\left[\frac{1}{3} - \frac{\alpha}{2} + \alpha^2 - \alpha^3 \ln\left(1 + \frac{1}{\alpha}\right)\right]} + \frac{3}{8} C (1 - p) \frac{1 + AR}{AR} \frac{L_m}{w} \right\}, \tag{10.30}$$

where

$$\alpha = \frac{L_m}{d} \frac{R_c}{1 - R_c}, \tag{10.31}$$

and where ρ_0 is the bulk resistivity, w is the wire width, AR is the aspect ratio (wire height divided by wire width), d is the average grain size (for relatively narrow wires this can be taken as the wire width), p is called the *specularity parameter* (relating to reflection from the wire surface), R_c is the grain boundary reflectivity coefficient, and C is a constant (taken to be 1.2 in this model). The first term is related to grain-boundary scattering, and the second term to wire-surface scattering. Both p and R_c can take values between 0 and 1, and typical values determined by fitting (10.30) to experimental results are $p = 0.3$–0.5 and $R_c = 0.2$–0.3. For example, using $p = 0.50$ and $R_c = 0.27$ we have $\sigma = 1.22 \times 10^7$ S/m for a 10×10 nm^2 copper wire (down from 5.9×10^7 S/m for the bulk value). The preceding model may work down to wire cross-sectional dimensions on the order of perhaps 5–10 nanometers, below which a quantum wire model that accounts for transverse quantization would be necessary.

However, as complicated as surface- and grain-boundary scattering are, other factors also determine the conductivity of a nanowire. For example, the I–V characteristic of a 30 nm radius, 2.4 μm long single-crystalline copper nanowire is shown in Fig. 10.4. In Fig. 10.4(a), the room temperature characteristics are shown, along with an SEM image of the wire contacting two Au electrodes. The resistance is approximately 10 times the value expected from (10.28) using σ for bulk copper. The difference could be due to electron scattering (as discussed earlier), large contact resistance between the electrodes and the wire, or surface oxidation. To consider the latter effect, in Fig. 10.4(b) the current–voltage characteristics of a 25 nm radius copper nanowire are shown for various times over a 12-hour period. The increasing oxidation of the copper resulted in the material becoming more like Cu_2O, and after complete oxidation, the wire acts like a p– type semiconductor.

Figure 10.5 shows the wire in Fig. 10.4(a) after complete oxidation, at both room temperature and 4.2 K. The Cu_2O wire creates a Schottky contact with each electrode, and so the I–V curve has a double-diode (back-to-back diode) behavior. Due to the large surface-to-volume ratio of nanostructures, these kinds of effects can be extremely deleterious to performance.

[†]See [27] and references therein.

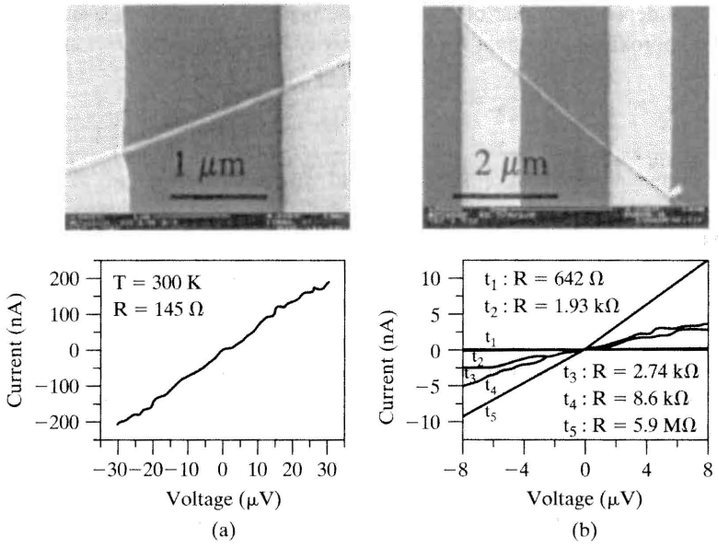

Figure 10.4 (a) Room temperature I–V characteristics of a 30 nm radius, 2.4 μm long single-crystalline copper nanowire. A SEM image of the wire contacting two Au electrodes is shown above the plot. (b) Current–voltage characteristics of a 25 nm radius copper nanowire for various times $t_1 < t_2 < t_3 < t_4 < t_5$ over a 12-hour period. The increasing oxidation of the copper resulted in the wire acting like a p– type semiconductor. (From Toimil Molares, M. E., et al., "Electrical Characterization of Electrochemically Grown Single Copper Nanowires," *Appl. Phys. Lett.* 82 (2003): 2139. © 2003, American Institute of Physics.)

10.2 BALLISTIC TRANSPORT

As the length L of a conduction path becomes very small, do the formulas (10.28) or (10.29) continue to hold? One may guess that they do not, since, for one thing, conductivity is a bulk parameter, and is derived assuming a large number of electrons (the electron gas model) and a large number of collisions between electrons and phonons, impurities, imperfections, etc. In particular, if L is reduced to become much less than the mean free path L_m, one would expect that no collisions would take place, rendering the collision-based model useless. This indeed occurs, and in this section, we consider the case when $L \ll L_m$.

It has been possible only recently to experimentally investigate resistance at the nanoscale. Much progress has been made in understanding the underlying physics of nanoscale and *mesoscopic*[†] transport. The overarching idea is that at very small length scales, electron transport occurs *ballistically*. It can be appreciated that ballistic transport will be important in many future nanoscopic devices.

[†]Mesoscopic refers to size scales between microscopic (atomic) and macroscopic (sizes of everyday objects). For example, carbon nanotubes are often mesoscopic, having nanometer radius values yet having anywhere from nm to cm lengths.

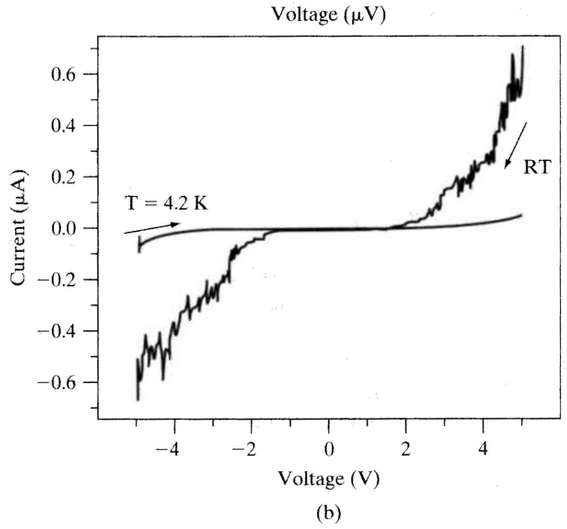

Figure 10.5 The Cu wire from Fig. 10.4(a) after complete oxidation. The Cu_2O wire acts like a p-type semiconductor, creating Schottky contacts with each electrode, and so the I–V curve has a double-diode (back-to-back diode) behavior. (Based on a figure from Toimil Molares, M. E., et al., "Electrical Characterization of Electrochemically Grown Single Copper Nanowires," *Appl. Phys. Lett.* 82 (2003): 2139. © 2003, American Institute of Physics.)

10.2.1 Electron Collisions and Length Scales

There are two types of collisions to consider. First, an electron can collide with an object such that there is no change in energy. (Think of a ball bouncing off of a fixed surface.) This type of collision is called an *elastic collision*, and typically, collisions between electrons and fixed impurities are elastic. In the second type of collision, the energy of the electron changes (although total energy is conserved). This type of collision is called an *inelastic collision*, and typically results from collisions between electrons and phonons (quantized lattice vibrations), or between electrons and electrons.

Considering the preceding discussion, we'll define several length scales.

- L is the system length, in this case the length of the conductor in question.
- L_m is the mean free path defined previously. However, now we want to be explicit and define this to be the length that the electron can travel before having an *elastic* collision.
- L_ϕ is the length over which an electron can travel before having an *inelastic* collision. This is also called the *phase-coherence length*, since it is the length over which an electron wavefunction retains its coherence (i.e., retains its phase memory). Over

the phase-coherence length, the phase of the wavefunction evolves smoothly. From (3.135),

$$\Psi(\mathbf{r}, t) = \psi(\mathbf{r})\, e^{-iEt/\hbar}, \tag{10.32}$$

assuming a time-independent potential. We see that elastic collisions do not disrupt phase coherence, but that inelastic collisions destroy phase coherence. These inelastic collisions are called *dephasing events*. Among other things, these dephasing events will destroy interference effects, including electrons interfering with themselves. L_ϕ is usually on the order of tens to hundreds of nanometers at low temperatures.

As is typical of nanosystems, thermal effects play an important role in phase coherence. This is obviously the case for electron-phonon collisions, since phonon energy will be greater at higher temperatures; in the classical model, the lattice vibrates more at higher temperatures. Furthermore, due to thermal energy, at nonzero temperatures, an electron should be represented by a wavepacket, the energies of which will vary on the order of $k_B T$. As T increases, obviously, the spread of energies will increase, along with their associated phase differences, eventually leading to thermal decoherence even in the absence of particle scattering.[†] Decoherence of any kind is one of the reasons for systems to exhibit classical behavior, and is one of the most problematic issues facing the development of quantum computers. That is, the computation must be finished before the quantum state decoheres (with some exceptions), and, at present, this time is quite short.

For simplicity, we will divide electron transport into two regimes:[‡]

- For $L \gg L_\phi, L_m$, we have *classical transport*, which is the familiar macroscopic case previously described. Ohm's law applies, and momentum and phase relaxation occur frequently as charges move through the system. Because of this, we cannot solve Schrödinger's equation over the whole conductor length L. It is fortunate that semiclassical or even classical models generally work well in this case.
- For $L \ll L_m, L_\phi$, we have *ballistic transport*, which is our main interest here. Ballistic transport occurs over very small length scales, and is obviously coherent; the electron doesn't "hit" anything as it travels through the material, and, therefore, there is no momentum or phase relaxation. Thus, in a ballistic material, the electron's wavefunction can be obtained from Schrödinger's equation.[§] One practical application of ballistic transport is to ultra-short-channel semiconducting FETs,[†] or carbon nanotube transistors. Short interconnects may exhibit ballistic transport properties, although material processing issues are important.

[†]One can also view thermal decoherence as an interaction between the object and its environment, since a "warm" object can emit photons (classically, blackbody radiation). Recent experiments have shown that thermal decoherence will result if the object/particle emits photons capable of resolving its path. Just as in the case of the double-slit experiment discussed in Chapter 2, observing the particle's path, such as which slit it goes through in a two-slit experiment, results in the object exhibiting classical behavior.

[‡]There are several other transport categories between the two extremes of classical and ballistic transport, although these won't be considered here.

[§]In principle, if there are scattering events at specific positions in space, then Schrödinger's equation can be applied to each region between the scatterers, and the solutions connected. This is similar to what is done for heterostructures (i.e., applying Schrödinger's equation region by region, and then connecting the solutions by the boundary conditions), although the scattering problem presents a much more difficult task.

10.2.2 Ballistic Transport Model

In the following discussion, we consider a wire having small width (in two dimensions) or diameter/cross section (in three dimensions), on the order of[‡] λ_F, and length $L \ll L_m, L_\phi$, oriented along the x coordinate, extending from $x = 0$ to $x = L$. We assume that at both ends of the there are *reservoirs* of electrons; these reservoirs are simply macroscopic metal contacts that act as infinite sources and sinks for electrons, as shown in Fig. 10.6.

First, concerning the reservoirs themselves, from (4.54), for example, if the reservoir has dimensions $D \times D \times D$, then electrons in the reservoir have energy

$$E_n = \frac{\hbar^2 \pi^2}{2mD^2} n^2, \tag{10.33}$$

and for D sufficiently large the energy states in the reservoirs form essentially a continuum, as in a classical model. It is this continuum that is the infinite source and sink for electrons.

The Ballistic Channel and Subbands. Not surprisingly, we need to return to the quantum mechanical picture to consider ballistic transport between the reservoirs. From the discussion of subbands in Sections 4.7.2 and 9.2, electrons in the wire will have energy

$$\begin{aligned} E &= \frac{\hbar^2}{2m_e^*}\left(k_x^2 + k_{y,n_y}^2 + k_{z,n_z}^2\right) \\ &= E_{n_y,n_z} + \frac{\hbar^2}{2m_e^*} k_x^2, \end{aligned} \tag{10.34}$$

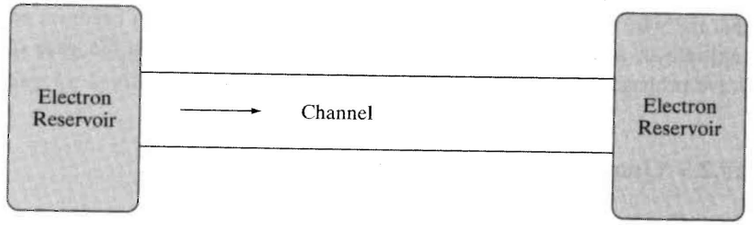

Figure 10.6 Ballistic channel connecting two electron reservoirs. The channel is parallel to the x-axis.

[†]For semiconducting channels, the specimen would need to be relatively pure, with low surface scattering, in order to achieve ballistic transport. Quasi-ballistic transport is more likely.

[‡]We assume a small cross section so as to have quantum confinement effects in the transverse direction; larger cross-section wires can be accommodated by a quasi-continuous, rather than discrete, energy level structure.

where k_x is the longitudinal wavenumber, which will be a continuous parameter (since electrons are free along the x coordinate), and the discrete indices n_y and n_z are subband indices. Subband energy levels are given by

$$E_{n_y,n_z} = \frac{\hbar^2}{2m_e^*}\left(k_{y,n_y}^2 + k_{z,n_z}^2\right), \tag{10.35}$$

where, for example, for an infinite confining potential (hard-wall case) and a rectangular cross-section ($w_1 \times w_2$) wire,

$$E_{n_y,n_z} = \frac{\hbar^2}{2m_e^*}\left(\left(\frac{n_y\pi}{w_1}\right)^2 + \left(\frac{n_z\pi}{w_2}\right)^2\right), \tag{10.36}$$

where $n_y, n_z = 1, 2, 3, \ldots$.

Let's assume that the quantum wire has a square cross section, such that $w_1 = w_2 = w$. Then, the hard-wall subband energy levels are given by

$$E_n = \frac{\hbar^2\pi^2}{2m_e^* w^2}n^2, \tag{10.37}$$

such that the number of subbands (also called the number of *electron channels*, or *modes*) at or below the Fermi energy is

$$N = \sqrt{\frac{E_F 2m_e^* w^2}{\hbar^2\pi^2}} = \frac{w}{\hbar\pi}\sqrt{E_F 2m_e^*} = \frac{wk_F}{\pi} = \frac{w}{\lambda_F/2}, \tag{10.38}$$

where we assumed the usual $E(k)$ relationship for electrons,

$$E = \frac{\hbar^2 k^2}{2m_e^*}. \tag{10.39}$$

Therefore, as the width of the wire increases, the number of electron channels increases, such that the wire gains a new channel (mode) each time the width becomes equal to an integral multiple of a half-Fermi wavelength. This is very similar to the case of electromagnetic wave propagation in a hollow conducting waveguide.

10.2.3 Quantum Resistance and Conductance

In order to further characterize ballistic transport, we need to determine the resistance of the channel. We assume that a potential V is applied across the two reservoirs in Fig. 10.6, positive on the left side, driving a current in the wire. The Fermi energy in the left reservoir is then $E_F - eV$, whereas in the right reservoir it is E_F. (We assume the left and right reservoirs are identical.) The electrons in the wire have wavefunction ψ,

$$\psi(x, y, z) = \psi_x(x)\,\psi_y(y)\,\psi_z(z), \tag{10.40}$$

with an associated probabilistic current density

$$\mathbf{J}(x, y, z) = \frac{\hbar}{m_e^*}\mathrm{Im}\left(\psi^*\nabla\psi\right). \tag{10.41}$$

The current in the wire is, from (3.190),

$$\begin{aligned} I_x &= \int_y\int_z (-e)\,\mathbf{J}(x, y, z)\cdot\mathbf{a}_x\, dydz \\ &= -\frac{e\hbar}{m_e^*}\int_y\int_z \mathrm{Im}\left(\psi^*\frac{\partial}{\partial x}\psi\right) dydz \\ &= -\frac{e\hbar}{m_e^*}\int_y\int_z |\psi_y(y)|^2\,|\psi_z(z)|^2\,\mathrm{Im}\left(\psi_x^*(x)\frac{\partial\psi_x(x)}{\partial x}\right) dydz \\ &= -\frac{e\hbar}{m_e^*}\mathrm{Im}\left(\psi_x^*(x)\frac{\partial\psi_x(x)}{\partial x}\right), \end{aligned} \tag{10.42}$$

where we used the normalization condition

$$\int_y\int_z |\psi_y(y)|^2\,|\psi_z(z)|^2\, dydz = 1. \tag{10.43}$$

Now, assume the wavefunction can be represented by a traveling state, indicating left-to-right (positive k) movement of the electron,

$$\psi_x(x) = \frac{1}{\sqrt{L}}e^{ikx}, \tag{10.44}$$

such that

$$I_x = -\frac{e\hbar}{m_e^* L}\mathrm{Im}\left(e^{-ikx}(ik)\,e^{ikx}\right) = -\frac{e\hbar k}{m_e^* L}. \tag{10.45}$$

Since this is the current due to a certain state, and since two electrons can fill each state (accounting for spin), then, multiplying by two, we obtain

$$I_{x,k} = -\frac{2e\hbar k}{m_e^* L}, \tag{10.46}$$

where the subscript indicates both the direction and the state dependence.

The preceding quantity, (10.46), is the current in the x-direction carried by electrons in state k. However, we do not know if a certain state will be filled. Furthermore, the probability that the electron makes it into the channel from the left reservoir, and out of the channel into the right reservoir, must be incorporated. The desired result is obtained by summing over all possible states (k) and all possible electron channels (the N subbands). For each state, we multiply by the Fermi–Dirac probability of the state k in the left reservoir being occupied,

$f(E, E_F - eV, T)$, the energy-dependent transmission probability of passing through the channel, $T_n(E)$, and the current carried by each state, $I_{x,k}$. The resulting current flowing from left to right is

$$I_{L\to R} = \sum_{n=1}^{N} \sum_{k} f(E, E_F - eV, T)\, T_n(E) \left(-\frac{2e\hbar k}{m_e^* L}\right) \tag{10.47}$$

$$= \sum_{n=1}^{N} \frac{L}{2\pi} \int_{-\infty}^{\infty} f(E, E_F - eV, T)\, T_n(E) \left(-\frac{2e\hbar k}{m_e^* L}\right) dk$$

$$= -\frac{2e}{h} \sum_{n=1}^{N} \int_{-\infty}^{\infty} f(E, E_F - eV, T)\, T_n(E)\, dE,$$

where the factor $L/(2\pi)$ comes about in converting the sum over k to an integral.† Since the transmission probability $L \to R$ is the same as that for $R \to L$ conduction (assuming a symmetric potential barrier and identical reservoirs),

$$I_{R\to L} = -\frac{2e}{h} \sum_{n=1}^{N} \int_{-\infty}^{\infty} f(E, E_F, T)\, T_n(E)\, dE, \tag{10.48}$$

and the total current flowing is

$$I = I_{L\to R} - I_{R\to L} = -\frac{2e}{h} \sum_{n=1}^{N} \int_{-\infty}^{\infty} \{f(E, E_F - eV, T)$$

$$- f(E, E_F, T)\}\, T_n(E)\, dE. \tag{10.49}$$

If eV is sufficiently small, then

$$f(E, E_F - eV, T) - f(E, E_F, T) \simeq \frac{\partial f(E, E_F, T)}{\partial E_F} (-eV) \tag{10.50}$$

$$= -\frac{\partial f(E, E_F, T)}{\partial E} (-eV),$$

resulting in

$$I = \frac{2e^2}{h} V \sum_{n=1}^{N} \int_{-\infty}^{\infty} \left(-\frac{\partial f(E, E_F, T)}{\partial E}\right) T_n(E)\, dE. \tag{10.51}$$

†For a free particle in one dimension, assuming periodic boundary conditions as discussed in Section 4.3.3, each state occupies a region of length $2\pi/L$ in k–space.

The current (10.51) leads to the temperature-dependent conductance

$$G(T) = \frac{I}{V} = \frac{2e^2}{h} \sum_{n=1}^{N} \int_{-\infty}^{\infty} \left(-\frac{\partial f(E, E_F, T)}{\partial E}\right) T_n(E)\, dE. \tag{10.52}$$

For very low temperatures, the Fermi–Dirac distribution resembles a step function,

$$\left(-\frac{\partial f(E)}{\partial E}\right) = \delta(E_F - E), \tag{10.53}$$

such that

$$G(T = 0) = \frac{2e^2}{h} \sum_{n=1}^{N} T_n(E_F). \tag{10.54}$$

As the width of the physical channel increases, there are more electronic conduction channels (subbands), as given by (10.38), increasing N.

From (10.54), if, for instance, there are N electronic channels, and if the transmission probability is one for each channel, then

$$G = \frac{2e^2}{h} N, \tag{10.55}$$

which is known as the *Landauer formula*. (Some of the preceding expressions could also be given this name.) Since N is the number of conduction channels, using (10.38) we have

$$G = \frac{2e^2}{h} \frac{2w}{\lambda_F} \tag{10.56}$$

for a wire with square cross section w^2. The resistance of each channel is

$$R_0 = \frac{h}{2e^2} = 12.9\ \text{k}\Omega, \tag{10.57}$$

which is known as the *resistance quantum* ($G_0 = 2e^2/h$ is called the *conductance quantum*), and the total resistance is

$$R = \frac{h}{2e^2 N} = \frac{12.9}{N}\ \text{k}\Omega. \tag{10.58}$$

As the number of channels increases (i.e., as N increases by increasing the size of the physical channel's cross section), conductance increases and resistance decreases (analogous to adding additional wires to a wire bundle). The classical theory also predicts this behavior (e.g., (10.28)), although the quantum theory shows that this happens in discrete steps, as the number of electron channels increases. As N gets very large, the electron channels essentially form a continuum, and the quantum theory tends towards the classical

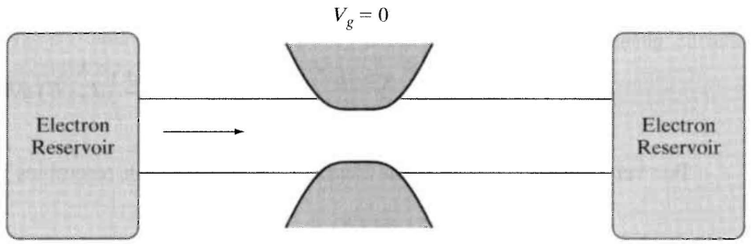

Figure 10.7 Two electron reservoirs connected by a ballistic channel. Channel width is controlled by the gate voltage applied at the gate electrodes. $V_g = 0$ and channel is relatively open.

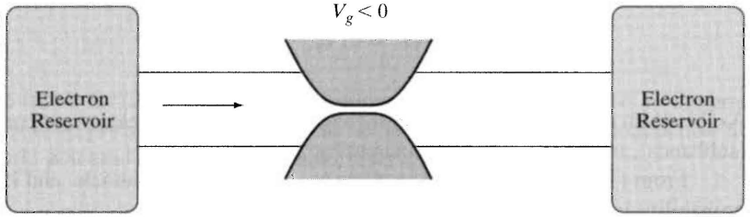

Figure 10.8 Same as Fig. 10.7, although with $V_g < 0$ so that the channel is constricted.

limit. However, in the presence of scattering, resistance quantization does not, in general, appear.[†]

The quantization of conductance is readily shown in low-temperature experiments. A schematic representation is shown in Figs. 10.7 and 10.8, where the left reservoir represents the source, and the right reservoir, the drain, and where a gate electrode is located near the center of the channel. The material between the source and drain is a two-dimensional electron gas (typically generated by a semiconductor heterojunction; see Section 9.1.1), such that when we apply a negative voltage to the gate, we deplete the carriers near to the gate, and constrict the channel. Such a structure is known as a *quantum point contact.*

When $V_g = 0$, the channel is open, and the number of electronic channels (subbands) are determined by the width of the physical channel (for example, using (10.36) in a hard-wall model). Say, for instance, that for a given maximum electron energy E, current is carried in N subbands. Then, the conductance will be $G = G_0 N$. As the gate voltage is increased in the negative direction, the physical channel is narrowed, as depicted in Fig. 10.8 resulting in larger spacing between subband energies by (10.36). In this case, fewer subbands

[†]It is worth noting that the general Landauer formula (10.54) applies to tunnel junctions as well, such as depicted in Fig. 6.2 on page 185 , resulting in

$$G = \frac{2e^2}{h} T(E_F), \tag{10.59}$$

where $T(E_F)$ is the transmission coefficient (6.15) obtained from solving Schrödinger's equation, evaluated at the Fermi energy.

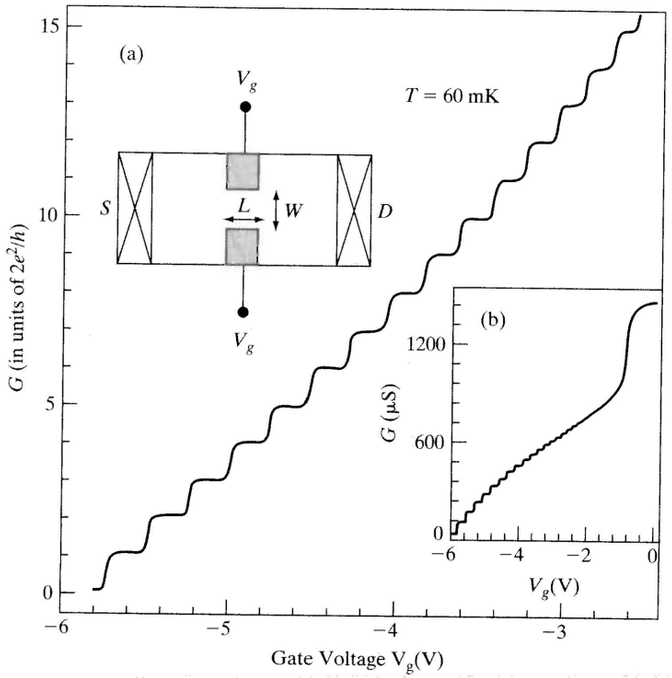

Figure 10.9 Conductance of a sample at $T = 60$ mK. Insert (a) shows a schematic of the split-gate device (not depicted is the electron gas connecting source and drain), and insert (b) shows the raw data. The width is 0.95 μm, and $L = 0.4$ μm. Although L and W are relatively large, ballistic transport occurs due to the low temperature, and commensurate long mean-free path. In this case, $\mu_e = 4.5 \times 10^6$ cm^2 V^{-1}s^{-1}. (Based on a figure from Thomas, K. J., et al., "Interaction Effects in a One-Dimensional Constriction," *Phys. Rev. B* 58 (1998): 4846. © 1998, American Physical Society.)

will be occupied, since only the subbands having $E_n \leq E$ will be populated (i.e., we hold E fixed while increasing the spacing between E_n levels). Thus, as the channel narrows, N decreases, and, therefore, the conductance decreases in integral units[†] of G_0. This forms the step-like behavior shown in Fig. 10.9.

Notice that as temperature increases, the observed quantization tends to vanish. This is due to thermal energy $k_B T$ becoming comparable to the subband energy spacing. For instance, at room temperature ($T = 293$ K), $k_B T \simeq 0.025$ eV. For a rectangular cross-section wire with infinite confining potential (hard-wall model), from (10.36) we have

$$E_{n_y,n_z} = \frac{\hbar^2}{2m}\left(\left(\frac{\pi n_y}{L_y}\right)^2 + \left(\frac{\pi n_z}{L_z}\right)^2\right). \tag{10.60}$$

[†]The observation of quantized conductance relies on assuming an *adiabatic* transition between the different regions, that is, that the transition is gradual enough not to engender scattering between subbands.

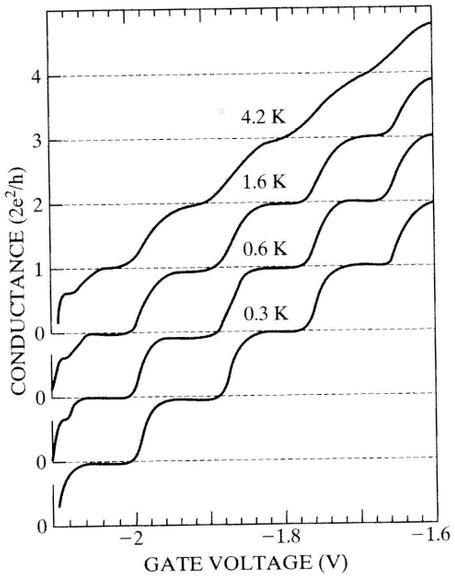

Figure 10.10 Temperature dependence of quantized conductance for a quantum point contact. The two-dimensional electron gas has a Fermi wavelength of 40 nm, and the width of the point contact is around 250 nm. (Based on Fig. 6 from van Wees, B.J., L.P. Kouwenhoven, E.M.M. Willems, C.J.P.M. Harmans, J.E. Mooij, H. van Houten, C.W.J. Beenakker, J.G. Williamson, and C.T. Foxon, "Quantum Ballistic and Adiabatic Electron Transport Studied with Quantum Point Contacts," *Phys. Rev. B* 43 (1991): 12431. © 1991, American Physical Society.)

Assuming $L_y = L_z = 10$ nm, then with $n_y, n_z = 1, 1$ and $n_y, n_z = 1, 2$ we have, $E_{1,1} = 0.0075$ eV and $E_{1,2} = 0.0188$ eV, such that $\Delta E = 0.0113$ eV, which is less then $k_B T$. Therefore, the subband quantization becomes "washed out." However, if $L_y = L_z = 1$ nm, then $E_{11} = 0.75$ eV and $E_{12} = 1.88$ eV, such that $\Delta E = 1.13$ eV, which is much greater than $k_B T$. In this case, the conductance quantization will be quite evident at room temperature. The temperature dependence of the conductance quantization of a quantum point contact is shown in Fig. 10.10, where quantization disappears quickly with increasing temperature due to the large size of the point contacts (around 250 nm).

Therefore, either temperature must be very low, or cross sections must be very small, for quantum effects to be noticed. Even for low temperatures, for paths longer than a few hundred nanometers, defects are likely to be present that destroy quantization.

Break Junctions. An interesting experiment involving break junctions can be performed to demonstrate the effect of conductance quantization in quantum wires. In a break junction, a wire having a relatively large radius is gradually pulled along the wire axis, and, as a result, the wire's radius becomes thinner as the wire stretches. Just before breaking, the wire's radius is on the order of an atom, and so at some point before breaking,

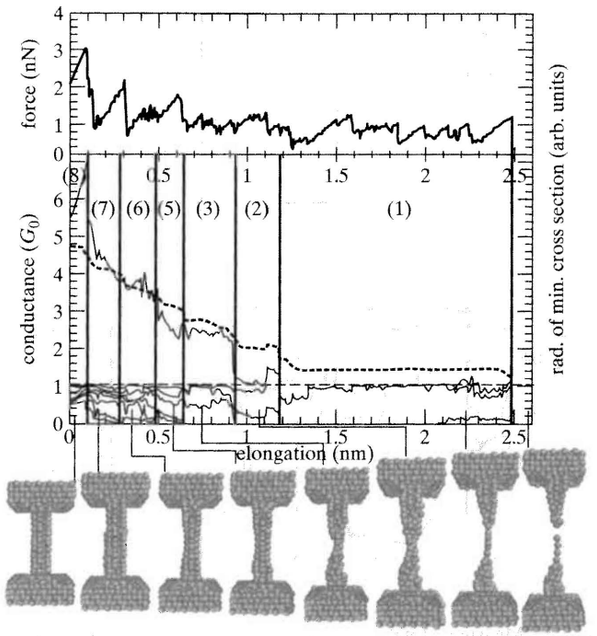

Figure 10.11 Theoretical simulation results from thinning a gold wire's radius by pulling the wire, at $T = 4.2$ K. The upper panel shows the strain forces as a function of the elongation of the contact. The middle panel shows the wire's conductance (solid line) and the radius of the minimum wire cross section (dashed line). The transmission coefficient of each channel is shown in the bottom panel. The vertical lines define regions with different numbers of open channels, ranging from 8 to 1. Breaking of the contact is depicted below the plot. (Based on a figure from Dreher, M.F., Pauly, J. Heurich, J.C. Cuevas, E. Scheer, and P. Nielaba, "Structure and Conductance Histogram of Atomic-Sized Au Contacts," *Phys. Rev. B* 72 (2005): 075435. © 2005, American Physical Society.)

one expects to see conductance quantization. These types of experiments have been widely performed, and quantization is indeed observed. In Fig. 10.11, the results of a molecular dynamics simulation are shown, and Fig. 10.12 provides measured results. In Fig. 10.11, elongation of the wire resulted in the formation of an atomic chain of gold atoms, reducing the number of channels to one.

Note that in these figures, the individual transmission coefficients of each channel are not generally unity, and so conductance values are not exactly integer multiples of G_0. Thus, the conductance (10.54) approximately applies to this case, rather than (10.55). For example, in Fig. 10.11, $G \simeq 2.4G_0$ when three channels exist, since the transmission coefficient of one of the channels is significantly below unity. Furthermore, although the number of modes decreases as the wire's radius decreases, at a given radius, the actual number of modes is a more complicated issue than given by the simple formula (10.38). This is due to the atomic structure of the wire when the wire's radius is reduced to only a few atoms.

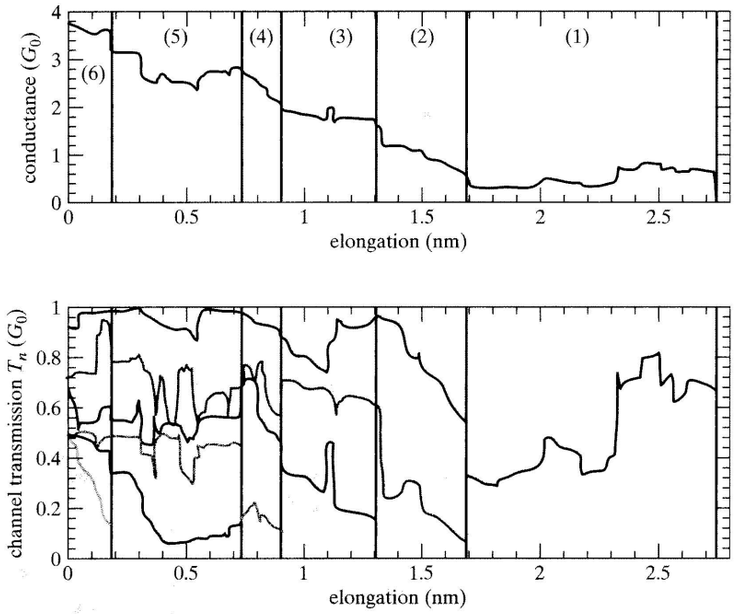

Figure 10.12 Measured total conductance of a gold wire (top panel) and the single-channel contributions (bottom panel) as a function of wire elongation. The vertical lines define regions with different numbers of channels, ranging from 6 to 1. Temperature was below 100 mK. (Based on a figure from Dreher, M.F., Pauly, J. Heurich, J.C. Cuevas, E. Scheer, and P. Nielaba, "Structure and Conductance Histogram of Atomic-Sized Au Contacts," *Phys. Rev. B* 72 (2005): 075435. © 2005, American Physical Society.)

10.2.4 Origin of the Quantum Resistance

Since $L \ll L_m, L_\phi$, there is generally no scattering along the conduction path, and we might have expected that the resistance of the channel would be zero (infinite channel conductance). That is, in our simple model, there are no collisions or interactions, and so there is no mechanism for energy dissipation. Therefore, there should not be any voltage dropped across the ballistic conductor, and, hence, resistance should be zero. However, the resistance obtained, (10.58), is not really the resistance of the channel, but of the contact between the physical channel and the electron reservoirs (similar to the junction between a large-diameter and small-diameter water hose). If the reservoirs are viewed as very wide material regions, one can think of them as having a large number of electronic channels. The small cross section physical channel has a small number of electronic channels, and so at the junction between the reservoir and the physical channel, there is a mismatch. Current passing through the reservoir, carried by the large number of electronic channels, must be redistributed among the small number of electronic channels available in the physically narrow channel, resulting in resistance. The resistance quantum, R_0, arises from perfect (infinitely wide) reservoirs in contact with a single electronic channel (i.e., a very narrow physical channel).[†] Indeed, one finds that the resistance of a ballistic channel is length independent, as long as $L \ll L_m, L_\phi$ is maintained. Furthermore, ballistic metal nanowires have been shown to be capable of carrying current densities much higher than bulk metals, due to the absence of heating in the ballistic channel itself.

10.3 CARBON NANOTUBES AND NANOWIRES

As discussed in Section 7.3.1, metallic carbon nanotubes are excellent conductors, and can exhibit d.c. ballistic transport over at least μm lengths. For an SWNT, when ballistic transport occurs, the resistance of the tube is length independent, and is, theoretically, approximately 6.45 kΩ. This resistance value results from having two propagation bands (called the π−bands) forming parallel propagation channels,[‡] where each channel has resistance equal to the resistance quantum, $R_0 \simeq 12.9$ kΩ. Thus,

$$G = \frac{2e^2}{h} N = \frac{4e^2}{h}, \tag{10.62}$$

$$R = \frac{h}{4e^2} = 6.45 \text{ k}\Omega. \tag{10.63}$$

Measurements on short tubes have verified this value, and values approaching (10.62) have been obtained in experiments on long tubes at lower temperatures. Note that, in contrast to solid metal quantum wires where the number of modes increase as the cross-sectional dimensions increase (e.g., (10.38)), for CNs the number of modes at the Fermi energy is two, independent of tube radius.

In practice, considerable care must be exercised to observe the resistance value 6.45 kΩ in carbon nanotubes, and, in fact, this is generally true in ballistic transport structures. The biggest experimental problem is to obtain sufficiently good (very low reflection) contacts to the tube, i.e., between the channel and the reservoirs. A multiwalled CN bridging two cobalt contacts is shown in Fig. 10.13.

In a metallic carbon nanotube the mean-free path is on the order of μm or more (often quoted values are in the range 1.3–1.7 μm) for low-bias voltages. The main source of resistivity for high-quality metallic CNs is scattering by acoustic phonons.[§] For lengths longer than the mean-free path, the resistance of a CN is length dependent. Several models

[†]Going in the other direction, we assume reflectionless contacts from the narrow physical channel to the large reservoirs.

[‡]If one wants to separate spin effects, carbon nanotubes can be considered to have four parallel channels (each of the two channels has two possible spin values), although in this case (10.55) becomes

$$G = \frac{e^2}{h} N \tag{10.61}$$

for an N channel system.

[§]Acoustic phonons are low-enegy phonons. The role of electron-phonon scattering in metallic carbon nanotubes is discussed in [22].

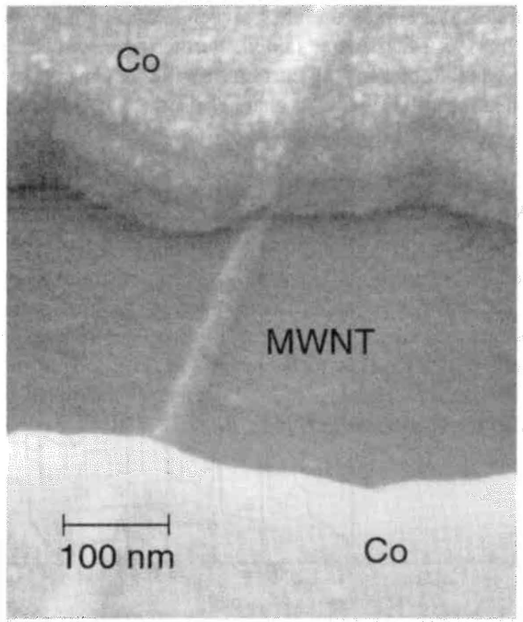

Figure 10.13 SEM image of a 15 nm radius MWNT bridging two cobalt contacts on an oxidized silicon wafer. The Co contacts lie on top of the MWNT; the image of the nanotube is seen through the Co layer due to the change in height of the evaporated film. This device was used for the study of spin transport (see the following section), although similar structures are used for d.c. and microwave charge transport characterization. (From Tsukagoshi, K., B.W. Alphenaar, and H. Ago, "Coherent Transport of Electron Spin in a Ferro Magnetically Contacted Carbon Nanotube," *Nature* 401 (1999): 572. Courtesy Macmillan Publishers Ltd. and Bruce Alphenaar.)

have been suggested, although in the low-bias regime (where voltages over the tube length are less than about one-tenth of a volt) a linear model,

$$R = \frac{h}{4e^2}\left(1 + \frac{L}{L_m}\right), \tag{10.64}$$

seems to work fairly at well least up to cm lengths. Figure 10.14 shows a plot of resistance versus tube length, where it can be seen that for longer tubes the resistance is approximately 6–7 $k\Omega$ per micron, in agreement with (10.64) if $L_m \simeq 1$ μm.

For high-bias voltages (above a few tenths of a volt) resistance becomes voltage dependent, and in typical SWNTs current tends to saturate around 25–30 μA. In high-quality tubes, this is mainly due to scattering with optical and zone-boundary phonons, which have energies on the order of 0.2 eV. This is because at high biases, electrons can gain enough energy to emit one of these phonons. In this case, the mean-free path can be as short as 10–30 nm. The length that an electron must travel to accelerate to this phonon

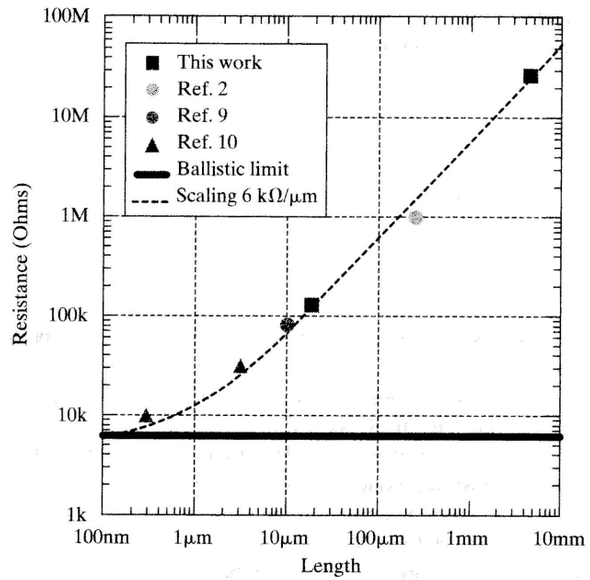

Figure 10.14 Resistance versus length for an SWNT. Symbols relate to the results from other work. All data are at room temperature. (Based on a figure from S. Li, Z.Y.C. Rutherglen, and P.J. Burke, "Electrical Properties of 0.4 cm Long Single-Walled Carbon Nanotubes," *Nano Lett.*, 4: 2003–2007, 2004. © 2004 American Chemical Society.)

range is[†]

$$L_h = \frac{E_{ph}}{e\,|\mathcal{E}|}, \tag{10.65}$$

where E_{ph} is the phonon energy and L_h is the high-bias mean-free path. Denoting the low-bias mean-free path by L_l, we see that *Matthiessen's rule* for combining mean free paths leads to

$$L_{mfp}^{-1} = L_l^{-1} + L_h^{-1}. \tag{10.66}$$

With this, CN resistance can be modeled by[‡] (10.64), leading to

$$R = \frac{h}{4e^2}\left(1 + L\left(\frac{1}{L_l} + \frac{1}{L_h}\right)\right) \tag{10.67}$$

$$= \frac{h}{4e^2}\left(1 + \frac{L}{L_l}\right) + \frac{h}{4e}\frac{L\,|\mathcal{E}|}{E_{ph}} \tag{10.68}$$

$$= R_{\text{low-bias}} + \frac{V}{I_0}, \tag{10.69}$$

[†]This is obtained from energy being equal to force multiplied by distance.
[‡]See, e.g., [23] and [24].

where $V = L\,|\mathcal{E}|$ and $I_0 = 4eE_{ph}/h$. For $E_{ph} = 0.2$ eV, $I_0 = 30$ μA. It is easy to see that with this model current saturates, since

$$I = \frac{V}{R_{\text{low-bias}} + \frac{V}{I_0}}, \tag{10.70}$$

and for $V/I_0 \gg R_{\text{low-bias}}$,

$$I = \frac{V}{\frac{V}{I_0}} = I_0. \tag{10.71}$$

Although CNs can be grown that are nearly atomically perfect, defects do occur. One estimate is that high-quality, SWTNs have, on average,† one defect per 4 μm, although far fewer defects are possible. While even one defect per 4 μm is quite a small number (approximately one chemical bond out of a trillion is out of place, on a par with high-quality Si), the presence of a single defect can significantly influence electronic properties. Being a one-dimensional conductor, essentially current can't flow around the defect.‡ The conductance of a carbon nanotube in the presence of defects can vary substantially from the defect-free case, and defects obviously impact ballistic transport in CNs. Not surprisingly, defects are found more often in areas of tube curvature. Furthermore, defects are chemically active sites on the tubes, and seem to play a strong role in the sensitivity of CNs as gas sensors.

10.3.1 The Effect of Nanoscale Wire Radius on Wave Velocity and Loss

One important aspect of carbon nanotubes, and seemingly of all nanoradius conductors, is that the velocity of wave propagation along the structure is quite slow compared with macro- and even micron-scale conductors. Recall that although electrons move relatively slowly inside a conducting material (at approximately v_F, which for copper is 1.57×10^6 m/s $= 0.0052c$), for good conductors, electrical signals propagate outside the material as electromagnetic waves guided by the conductor. Therefore, wave velocities are approximately the speed of light in the medium outside of the wire. Assuming that $\mu_r = 1$, which is the usual case, we find that this velocity is given by $c/\sqrt{\varepsilon_r}$. Thus, for wires surrounded by free space, $v = c \simeq 3 \times 10^8$ m/s, and since ε_r for typical dielectric materials is in the range 1–10, signal propagation is usually close to c. This conclusion holds for macro- and micron-scale radius conducting wires and circuit traces.

However, as the radius of metal wires/interconnects decreases to the nanoscale, the signal velocity of the wave guided by the wire slows significantly. For example, Fig. 10.15 shows the normalized phase velocity of electromagnetic wave propagation, $s_r = v_p/c$, for an infinite carbon nanotube (radius $a = 2.712$ nm) and for various solid round copper wires

†See [13].

‡This is a general property of nanoscale devices; a very small number of defects, or a small amount of stray charge, can sometimes significantly affect device behavior.

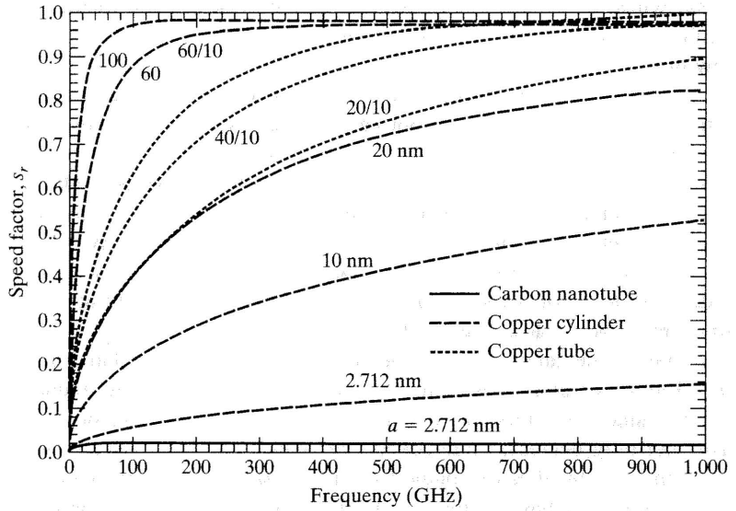

Figure 10.15 Predicted speed factor $s_r = v_p/c$ for wave propagation along an infinite carbon nanotube, and for various solid round copper wires and hollow copper tubes. For the CN and solid wires, a denotes the radius. For the tubular wires, results are labeled as a/d, where a is the outer radius and d is the tube wall thickness. (Based on a figure from Hanson, G.W. "Current on an Infinitely-Long Carbon Nanotube Antenna Excited by a Gap Generator," *IEEE Trans. Antennas Propagat.* 54 (2006): 76–81. © 2006, IEEE.)

and hollow copper tubes.† For the tubular wires, results are labeled as a/d, where a is the outer radius and d is the tube wall thickness. Results are for a single wire or tube in free space, i.e., no ground plane is present.

It can be seen that for relatively large radius copper wires, say, $a = 100$ nm or above, wave velocity is close to c, but for smaller radius wires and tubes, wave velocity is significantly decreased. Nevertheless, the carbon nanotube has the slowest wave velocity (although accounting for the decrease in copper conductivity at nanoradius values could change this conclusion). Theoretical analysis predicts that for waves guided by the CN, electromagnetic wave velocity is on the order of the Fermi velocity for electrons on the tube, $v_F \simeq 9.71 \times 10^5$ m/s. Different estimates yield the range $v_p \simeq 2v_F - 6v_F$, although all methods agree that wave velocity is quite slow, being several orders of magnitude below c. For example, assuming $v_p = 3v_F$, we have $v_p = 0.01c$. Given that interconnect delay presents a major bottleneck in chip performance, this slow speed is unfortunate (although, from Fig. 10.15, the same can be said about nanoradius copper interconnects). Signal propagation velocity can be increased by using larger-radius

†In Fig. 10.15, the results for the copper wires were obtained using the frequency-dependent conductivity of bulk copper. As described in Section 10.3.1, due to grain-boundary and surface scattering, impurities, and various fabrication aspects, the conductivity of nanoradius copper wires significantly decreases from the bulk value, and would tend to further slow wave propagation. However, the bulk value for copper conductivity is used here, since more realistic high-frequency values are not available.

metal wires, or by using, say, bundles of nanotubes, although this also brings about difficulties in connecting these larger-sized interconnects to devices having dimensions of a few nm.

However, signal speed is not the only figure of merit. Although the topic of IC interconnect performance will not be discussed in detail here, resistance and wire loss are obviously important. Considering again a single tube or wire in free space (as in Fig. 10.15) having $a = 2.712$ nm, it has been shown that a typical SWNT suffers roughly three times less power attenuation than a solid copper cylinder having the same radius,[†] even assuming the bulk value of conductivity for copper, which is unreasonably optimistic. Decreasing the conductivity by a factor of 10 from the bulk value, which is still probably not enough of a decrease to account for the small radius of the wire, we find that the copper wire has 10 times more power loss than the CN.

Of course, attenuation can be greatly reduced by using larger radius metal wires, say, $a \sim 100$ nm or more. Also, bundles on nanotubes can be used, reducing the resistance via (10.58), since each tube can be considered to add two propagation channels to the bundle. This not only decreases interconnect resistance and loss, but also increases speed, to the point that CN bundles can outperform larger-radius copper interconnects.[‡] However, again it should be emphasized that to attach an interconnect to a nanoscopic circuit one may need to use interconnects with radius values on the order of several nm, and large-radius wires or bundles consisting of a large number of CNs may not be appropriate. Another consideration is that many nanoelectronic devices have high impedance (say, a tunneling device), and using a high impedance interconnect such as a single carbon nanotube may make impedance matching easier.

In summary, for nanoscale radius interconnects, a case can be made that carbon nanotubes seem to be superior to metal wires having similar radius values. This is due, in large part, to the difficulties in fabricating high-quality metal traces at the nanoscale (i.e., obtaining nanoradius metal interconnects that have material properties close to the bulk value). In contradistinction, high-quality CNs can be fabricated that are nearly defect free, and that perform close to their theoretical limits, although high-throughput volume manufacturing of electronic devices based on CNs is currently not possible.

10.4 TRANSPORT OF SPIN, AND SPINTRONICS

So far, the transport discussed in this chapter has been the transport of charge, and the electronics described in the preceding chapters have been based on charge. However, as described in Chapters 2 and 3, quantum particles also have spin. Unlike charge, spin is a purely quantum phenomenon, yet like charge, spin can be transported and/or used to store information. Devices based on spin (spin-based electronics, or *spintronics*) make up an important recent class of electronic devices. Current commercial applications include mass-storage devices such as hard drives, although logic and transistor applications, quantum computing technology, and a host of other applications are envisioned.

[†]See [12].

[‡]See [9], [24]

10.4.1 The Transport of Spin

A discussion of spin transport necessitates a discussion of magnetic materials. Although an everyday phenomenon, the theory of magnetism is extremely complicated, and in the following discussion, only a brief outline of the main ideas relevant to the transport of spin is provided.

The origin of magnetism is the orbital motion and spin of subatomic particles, with electrons being particularly important. It should be noted that all materials have some magnetic properties, and yet most materials are essentially nonmagnetic. That is, most materials have a very weak response to a magnetic field.

Materials can be divided into five basic groups according to the alignment of the magnetic moments of their atoms (due to orbital and spin momentum (Section 3.6)) in the presence of a d.c. magnetic field. Upon applying a magnetic field to a material, we find that the magnetic moments of the atoms tend to become oriented, inducing a net magnetization. Then, after the applied field is removed, this net magnetization may remain or disappear.

For example, in a *diamagnetic* material (DM), the induced magnetization disappears after the magnetic field is removed. That is, the net magnetic moment of an atom in a DM, due to orbital and spin momentum, is zero in the absence of an applied magnetic field. Application of a magnetic field produces a force (the Lorentz force, (3.212)) on the orbiting electrons, perturbing their angular momentum and creating a net magnetic moment. The resulting induced magnetic moments tend to oppose the direction of the applied field,[†] resulting in a relative permeability $\mu_r \simeq 0.9999$. Thus, diamagnetism is a very weak effect. Elements such as Ag and Pb are diamagnetic.

In a *paramagnetic* material (PM), atoms have a small net magnetic moment due to incomplete cancellation of the angular and spin momentums. Application of a magnetic field tends to align the magnetic moments in the direction of the applied field, resulting in $\mu_r \simeq 1.00001$. Thus, paramagnetism is also a very weak effect; for example, Al is paramagnetic. The overwhelming majority of materials are either diamagnetic or paramagnetic,[‡] and the effect is usually so weak that one often refers to these materials as nonmagnetic. This is why, unlike relative permittivity ε_r, which is almost always different than unity for materials, relative permeability $\mu_r \simeq 1$ is assumed for most materials. Note that a magnet will weakly attract PMs, and weakly repel DMs.

If the induced magnetization remains after the applied magnetic field is removed, the material is called a ferromagnetic material (FM). However, one does not necessary need to apply a magnetic field to align the magnetic moments in an FM—they may already be aligned. Ferromagnetism is the underlying principle of what one typically thinks of as a magnet. Ferromagnetic elements include Co, Fe, Ni, and their alloys, and these materials usually have[§] $\mu_r \gg 1$. Ferromagnetic materials become paramagnetic above a temperature known as the *Curie temperature*, which is above 600 K for Co, Fe, and Ni.

[†]In electromagnetics, this is known as *Lenz's law*.

[‡]All materials actually have a diamagnetic effect mainly from orbital motion of electrons, although often the diamagnetic effect is hidden by a slightly larger paramagnetic effect, or by a much larger ferromagnetic effect.

[§]However, this is an oversimplification, since relative permeability is usually nonlinear ($\mu = \mu(\mathbf{H})$, where $\mathbf{H}$ is the magnetic field intensity), and hysteric, and typically needs to be specified by a tensor since its value is different in different directions in the material.

Another class of materials is *antiferromagnetic*, such as chromium, Cr, below about 475 K, MnO, FeO, and others. These have ordered magnetic moments, although adjacent magnetic moments are antiparallel. A final category, *ferrimagnetic* materials (called *ferrites*, which are really compounds such as Fe_3O_4), have adjacent magnetic moments antiparallel but unequal. A depiction of the magnetic moments for the latter three material types is provided in Fig. 10.16.

In general, we are most interested in spin transport in FMs, or between ferromagnetic and nonmagnetic materials. In an FM, electronic current flow can be envisioned as occurring in two channels, one for spin-up electrons and the other for spin-down electrons. The density of states at the Fermi energy of the two channels differs in most ferromagnetics. Often the density of states for spin-up and spin-down electrons is nearly identical, but the states are shifted in energy, as depicted in Fig. 10.17.

The electrons having spin corresponding to the larger density of states at E_F are called the *majority carriers* (majority spin electrons), whereas the other spin electrons are called *minority carriers*. Each channel can be characterized by a conductivity ($\sigma_\uparrow$ for spin-up electrons, and $\sigma_\downarrow$ for spin-down electrons), and due to the asymmetry of the DOS for ferromagnetics, one channel will be dominant. That is, either $\sigma_\uparrow > \sigma_\downarrow$ or $\sigma_\uparrow < \sigma_\downarrow$ will occur. The most extreme example of asymmetry in the DOS is a *half-metallic ferromagnet*, which has only one spin channel (i.e., the density of states at the Fermi level is empty for one spin); an example is chromium dioxide, CrO_2. On the other hand, a nonmagnetic material has equal spin channels, as depicted in Fig. 10.17(a). The inherent asymmetry of spin channels in ferromagnetic materials means that they can be used as sources of spin-polarized currents.

Given the two-channel model for a ferromagnetic material, we can consider what happens when a spin-dominant electrical current passes from a ferromagnetic to a nonmagnetic material. (By nonmagnetic we actually mean a paramagnetic or diamagnetic material, obviously.) Consider the junction depicted in Fig. 10.18. On the FM side, there is strong

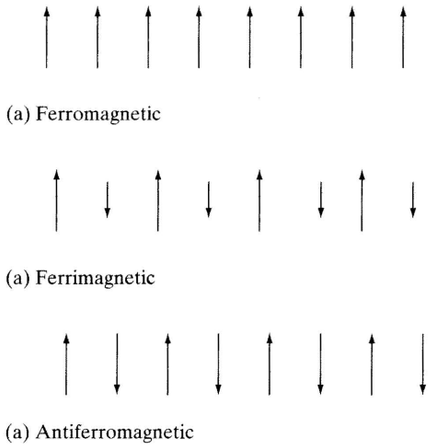

Figure 10.16 Depiction of the magnetic moments in (a) ferromagnetic, (b) ferrimagnetic, and (c) antiferromagnetic materials.

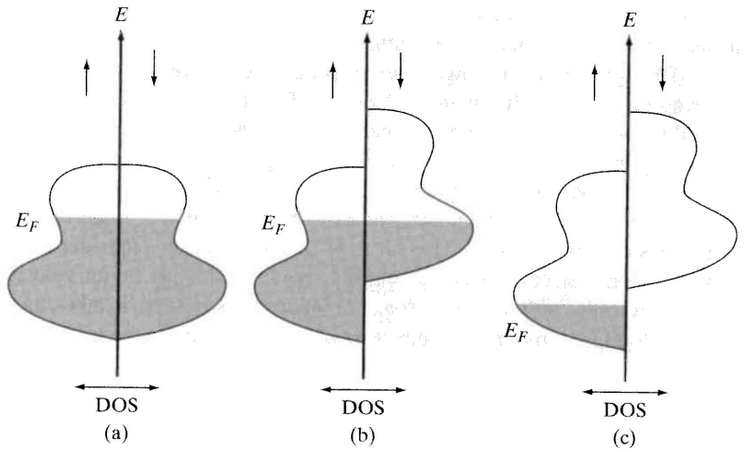

Figure 10.17 Density of states for spin-down electrons (indicated by the downward arrows), and for spin-up electrons (indicated by the upward arrows) for (a) a nonmagnetic material, (b) a ferromagnetic material, and (c) a half-metallic ferromagnet. A key parameter is the density of states at the Fermi energy.

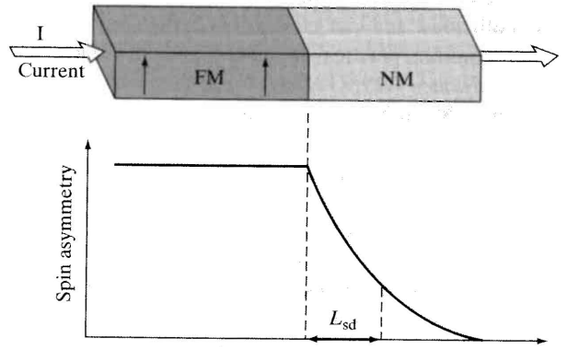

Figure 10.18 Depiction of spin asymmetry relaxation at the interface between a ferromagnetic and nonmagnetic material.

spin asymmetry. On the nonmagnetic material side, far from the interface, electrons will be carried in equal spin channels (assuming the nonmagnetic material is a conductor; if it is an insulator, there will be no current at all), and so there must be a region near to the interface where spin asymmetry decreases, as shown in the figure.

Spin is said to accumulate near the interface, and spin polarization decays exponentially away from the interface due to *spin-flip scattering events* on the scale of what is called the *spin diffusion length*, L_{sd}. Thus, spin-flip scattering events destroy the transport of spin,

leading to a characteristic length. This is analogous to momentum scattering events that lead to the concept of the mean free path.

The spin diffusion length can be roughly estimated as follows. Consider that, upon entering the nonmagnetic material from the FM, any given electron will undergo a number of collisions (say, N) before flipping its spin. These collisions are the same as described previously in Section 10.1, so that the average distance between collisions is the mean-free path, L_m. Without going into the details of current diffusion, it can be shown that the average distance that spin penetrates into the nonmagnetic material is[†] $L_m\sqrt{N/3}$, which is the desired spin diffusion length L_{sd}. To eliminate N, consider that the total distance traveled by the electron is $NL_m = v_F\tau_{\uparrow\downarrow}$, where v_F is the Fermi velocity of electrons and $\tau_{\uparrow\downarrow}$ is called the *spin-flip time* (i.e., the characteristic time it takes an electron to flip its spin, analogous to the momentum relaxation time τ for charge transport). Therefore,

$$L_{sd} = \sqrt{\frac{v_F\tau_{\uparrow\downarrow}L_m}{3}}. \tag{10.72}$$

Typical values of L_{sd} are on the order of several hundred nm, with spin-flip times on the order of tens of picoseconds (ps) at room temperature. In comparison, the typical mean free path in metals is on the order of tens of nm (e.g., for copper at room temperature, $L_m \simeq 40$ nm), and momentum relaxation times are on the order of a hundredth of a ps (e.g., for copper, $\tau = .025$ ps). Thus, spin polarization is preserved for a relatively long time and over relatively large distances. However, impurities in the nonmagnetic material will increase collisions, and can greatly lessen the spin diffusion length.

The most common practical application of spin polarization involves what is called the *giant magnetoresistance* (GMR) effect. It can be most easily understood by considering two layers of the same FM, such as Co, separated by a very thin (on the order of nm) nonmagnetic conducting spacer material, such as Cu. The geometry is depicted in Fig. 10.19.

Each ferromagnetic layer has a magnetization vector $\mathbf{M}$, and when these vectors are parallel,[‡] an electrical current can pass through the device. This is due to several reasons. First, since the spacer layer is thin (much thinner than the spin-diffusion length), spin can diffuse across the spacer to reach the other FM. Since that material's magnetization is parallel to the magnetization of the first layer, the density of states for those spin electrons is relatively high, and so there is low scattering. Thus, the flow of electrons can occur, resulting in a low electrical resistance. However, if the magnetization vector of the second FM is antiparallel with that of the first material, the majority-spin electrons see a small density of states in the second magnetic layer, and spin scattering is high. This is reflected by a much larger resistance to current flow,[§] depicted in Fig. 10.19. This resistance to current flow is called *magnetoresistance*, and the percentage ratio of the large and small resistance values is called the *GMR ratio*. Devices have been demonstrated with very high GMR ratios

[†]This comes from the theory of *random walks*, where the mean square distance that a particle moves in executing N steps of a random walk, with mean free path L_m, is NL_m^2.

[‡]We assume that the magnetization vectors can be set to be parallel or antiparallel by external magnetic fields.

[§]In the limiting case of two ideal half-metallic ferromagnets, if the magnetizations are antiparallel, resistance is infinite since the density of states in the last layer is empty for the electrons spin polarized from the first layer.

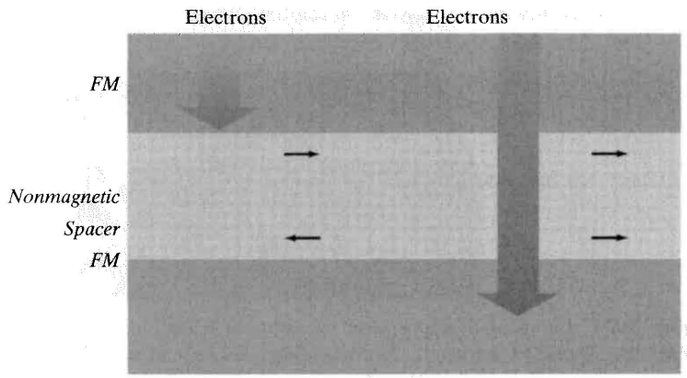

Figure 10.19 Depiction of the GMR effect. Two layers of FM are separated by a thin conducting (nonmagnetic) spacer. When the magnetization vectors in the two layers are parallel, an electrical current can easily pass through the device. If the magnetization vectors are antiparallel, then the resistance to current flow is much higher.

(hence the term "giant" in giant magnetoresistance), on the order of several hundred percent, although typical values are much less. Of course, this is a simplistic description, and various interface effects also play a role in the resistance obtained in such devices.

It should also be noted that current flow parallel to the layers is possible, and GMR can be obtained. In this case, however, the mean-free path is the important length parameter, and the GMR effect relies on the different mobilities of the spin-up and spin-down electrons, which are related to the two different densities of states. The non-magnetic layer is sufficiently thin (less than the mean-free path) so that current flow is spread across the multiple magnetic layers. If the layers have antiparallel magnetizations, each spin type will experience heavy scattering in one of the layers, resulting in relatively large resistance. However, if the layers have parallel magnetizations, one spin type will be heavily scattered in both layers, and the other spin type will experience little scattering, and a low resistance will result.

A related effect is when the spacer layer is insulating, and very thin. Electrons can tunnel through the insulating layer (spin is generally conserved in tunneling), and it can be considered that tunneling of spin-up and spin-down electrons are independent processes forming two independent spin tunneling channels. If the two ferromagnetic films are magnetized parallel to each other, the minority-spin electrons tunnel to minority states in the second ferromagnetic layer, and the majority-spin electrons tunnel to the majority states. If the two ferromagnetic layers have antiparallel magnetizations, the majority-spin electrons must tunnel to the minority states in the other layer. This forms a *magnetic tunnel junction*, the resistance of which (called the *tunneling magnetoresistance*) depends on the orientation of the two magnetization vectors and the spins of the incident electrons.

10.4.2 Spintronic Devices and Applications

A very important device based on the GMR effect is called the *spin valve*, depicted in Fig. 10.20.

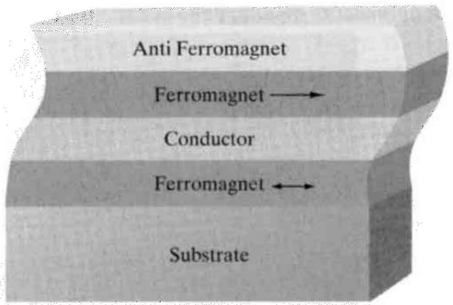

Figure 10.20 Depiction of a spin valve. (Courtesy of WTEC Inc. and Dr. James M. Daughton/NVE Corporation. Based on a graph by Professor Eshel Ben-Jacob.)

In this case, one of the ferromagnetic layers has a fixed (pinned) magnetization direction, due to the presence of the antiferromagnetic layer, and the other ferromagnetic layer magnetization is free to rotate upon application of a magnetic field (depicted by the double-headed arrow). An applied field, perhaps due to a magnetic bit on a hard drive, rotates the magnetization vector of the free layer, and when the two magnetization vectors are aligned, a minimum in device resistance is achieved. When the applied magnetic field results in antiparallel magnetization vectors, resistance of the device is greatly increased. Because of the strong GMR effect, GMR-based devices can be used as extremely sensitive magnetic read heads, allowing the storage capacity of a hard disk to increase considerably. Since the introduction of GMR read heads in 1997, hard disk density has increased greatly each year. Nearly all hard disk drives currently incorporate GMR read heads.

Mention must also be made of spin-based transistors. Considering the three layer structures already examined (i.e., ferromagnetic-nonmagnetic-ferromagnetic), it is not hard to envision adding a gate contact to the middle layer and forming a three-terminal transistor-like device, either in bipolar or field effect form. The middle layer may be made from a variety of materials, from normal metals to semiconductors, and applications of other materials, such as ferromagnetic semiconductors, are being activity considered. Furthermore, spin transistors have even been proposed using nonmagnetic semiconducting heterostructures, although in all cases there are many technological issues to be dealt with before spin-based transistors could be commercially viable. Other applications in spintronics include solid-state nonvolatile memories (since in many cases, spin states are retained after power is removed) and quantum information processing and quantum computation.

10.5 MAIN POINTS

In this chapter, we have considered classical and ballistic transport in materials, and the transport of spin. In particular, after studying this chapter, you should understand

- the classical theory of electrical conduction, including the concepts of conductivity and mobility, and the role of scattering;
- the semiclassical (Fermi) model of conductivity, and the idea of resistance;

- the idea of ballistic transport, including the various length scales (mean-free path, decoherence length, etc.) that define different transport regimes;
- the quantization of conductance and resistance;
- ballistic transport on CNs;
- size-dependent effects in nanowires;
- the basic ideas of spintronics, including the GMR effect and the operating principle of spin valves.

10.6 PROBLEMS

1. Compare the thermal velocity at room temperature with the Fermi velocity for a one-dimensional conductor having $N = 2 \times 10^7$ electrons/cm.
2. Determine the drift velocity for an electron in a material having momentum relaxation time $\tau = 2 \times 10^{-13}$ s, for an applied electric field $|\mathbf{E}| = 100$ V/m. If there are 3.4×10^{22} electrons per cm^3, what is the conductivity?
3. Another method to obtain electron drift velocity follows from the usual treatment of elementary differential equations modeling mass-spring systems; we can account for the effect of collisions by including a damping term in (10.5), resulting in

$$m_e \frac{d\mathbf{v}_d}{dt} + \frac{m_e \mathbf{v}_d}{\tau} = q_e \mathbf{E}. \tag{10.73}$$

   Solve (10.73) to determine the frequency-dependent version of the conductivity (10.12), assuming time-harmonic conditions.

   Comparing with the usual frictional term in a damped mass-spring system, we find that m_e/τ is analogous to a coefficient of friction. It is easy to see that (10.8) is a solution of (10.73).
4. Consider a two-dimensional electron gas in GaAs, with $n = 10^{12}$ cm^{-2}, and mobility 8, 200 cm^2/Vs. Determine the mean-free path from the semi-classical model, using $0.067m_e$ as the effective mass of electrons in GaAs.
5. We can consider a thin metal sheet as being two-dimensional if the thickness of the sheet, d, is sufficiently small such that we can ignore electron movement perpendicular to the plane of the sheet. One way to assess this issue is to compare the two-dimensional Fermi energy, $E_F^{(2d)}$, given by (8.39), with the energy ΔE required to excite an electron above the ground state in a one-dimensional hard-wall quantum well of size d. Using (4.35) we find that,

$$\Delta E = E_2 - E_1 = \frac{\hbar^2 \pi^2}{2m_e d^2} \left(2^2 - 1^2\right)^2. \tag{10.74}$$

   If $\Delta E \gg E_F$, the metal sheet is approximately two dimensional. This comparison is meaningful since the most important electrons will have energy equal to the Fermi energy, and if movement perpendicular to the plane of the sheet is to take place, the electrons must gain enough energy to move to a higher (perpendicular) state.

(a) Consider copper having $N_e \simeq 8.45 \times 10^{28}$ /m^3, such that the two dimensional density of electrons is approximately $N_e^{2d} = N_e^{2/3} = 1.93 \times 10^{19}$ /m^2. If the sheet thickness is $d = 0.2$ nm, is the sheet approximately two dimensional?

(b) Repeat (a) for a sheet with $d = 0.7$ nm.

6. One can approximately ignore quantization, and treat a layer of material as being three dimensional, if the (three-dimensional) Fermi wavelength is small compared with the sheet thickness d. Assuming we require

$$\lambda_F \leq 10d \tag{10.75}$$

in order to ignore quantization, determine the required sheet thickness that a copper sheet should have in order to be able to treat it as three dimensional. Repeat for n-type doped Si, assuming $N \simeq N_d = 1.5 \times 10^{16}$ cm^{-3}.

7. Do problems 10.5 and 10.6 provide self-consistent criteria for when a thin sheet can be considered to be two dimensional?

8. Using (10.30) with $p = 0.49$, $R_c = 0.27$, and d equal to wire width w, plot ρ as a function of wire width for a square cross-section copper wire.

9. A conducting wire carrying a signal is surrounded by teflon ($\varepsilon \simeq 2.5\varepsilon_0$). If the signal generates an a.c. 10 V/m electric field, thereby accelerating electrons, what is the approximate velocity of signal propagation?

10. Figures 10.1 (page 322) and 10.2 (page 323) show the Fermi surface in momentum space for a material. Draw a similar picture for a one-dimensional conductor.

11. Consider two concentric spherical conducting shells. The inner shell has radius a, the outer shell has radius b, and the material between the shells has conductivity σ. If the outer shell is grounded, and the inner shell is held at potential V_0, then elementary electrostatics shows that the resulting electric field in the space between the shells is[†]

$$\mathbf{E}(r) = \mathbf{r}\frac{V_0}{\frac{1}{a} - \frac{1}{b}}\frac{1}{r^2}. \tag{10.78}$$

Using this electric field, determine the resistance R seen between the two shells using (10.27).

[†]To derive (10.78), solve Laplace's equation,

$$\nabla^2 V = \frac{1}{r^2}\frac{\partial}{\partial r}\left(r^2\frac{\partial V}{\partial r}\right) = 0 \tag{10.76}$$

subject to $V(a) = V_0$ and $V(b) = 0$, then compute the electric field as

$$\mathcal{E} = -\nabla V = -\mathbf{r}\frac{\partial V}{\partial r}. \tag{10.77}$$

12. In Chapter 5, it was stated that collisions are necessary to frustrate Bloch oscillations, otherwise a d.c. voltage would result in an a.c. current. In this chapter, we have learned that if no collisions take place because $L \ll L_m, L_\phi$, d.c. ballistic transport will occur. These two facts seem to be in contradiction. Why are they not?

13. Consider a 20 nm length of a ballistic conductor, carrying $N = 4$ electron modes. Determine the current that will flow if a 0.3 V potential difference is applied across the length of the conductor. Assume low temperature, and that $T_n = 1$.

14. Consider a 5 nm length of a ballistic conductor, having square cross section of side 1 nm. If $E_F = 3.5$ eV, and $m^* = m_e$, determine the current that will flow if a 0.2 V potential difference is applied across the length of the conductor. Assume low temperature.

15. Consider a 50 nm length of a ballistic conductor, having square cross section of side 0.8 nm. If $E_F = 2.5$ eV, $m^* = m_e$, determine the current that will flow if a 0.2 V potential difference is applied across the length of the conductor. Assume low temperature.

16. Describe the difference between the physical channel and electronic channels in a quantum wire.